

Direction selectivity is computed by active dendritic integration in retinal ganglion cells

Benjamin Sivyver & Stephen R Williams

Active dendritic integration is thought to enrich the computational power of central neurons. However, a direct role of active dendritic processing in the execution of defined neuronal computations in intact neural networks has not been established. Here we used multi-site electrophysiological recording techniques to demonstrate that active dendritic integration underlies the computation of direction selectivity in rabbit retinal ganglion cells. Direction-selective retinal ganglion cells fire action potentials in response to visual image movement in a preferred direction. Dendritic recordings revealed that preferred-direction moving-light stimuli led to dendritic spike generation in terminal dendrites, which were further integrated and amplified as they spread through the dendritic arbor to the axon to drive action potential output. In contrast, when light bars moved in a null direction, synaptic inhibition vetoed neuronal output by directly inhibiting terminal dendritic spike initiation. Active dendritic integration therefore underlies a physiologically engaged circuit-based computation in the retina.

Electrophysiological recording and imaging techniques have demonstrated that local computational operations are executed in the dendritic tree of many classes of central neuron through the engagement of active dendritic integration^{1,2}. For example, in cortical pyramidal neurons maintained *in vitro*, local dendritic spikes, mediated by dendritic voltage-gated ion channels and synaptic mechanisms, can be generated in response to excitatory synaptic input at sites throughout the dendritic tree^{3–11}. Dendritic spikes amplify the effect of synaptic input on action potential output, providing a substrate for multi-layered and correlation-based integrative operations^{3,10,12–14}. However, it remains largely unknown how active dendritic integration contributes to the generation of defined neuronal and circuit-based computations, partly because of the difficulty of directly recording dendritic activity in functionally active neuronal circuits.

The retina offers an attractive system to investigate the role of active dendritic integration in neuronal circuit computation. The intact retinal network can be maintained *in vitro*, where it retains responsiveness to visual stimuli¹⁵. The output neurons of the retina, retinal ganglion cells (RGCs), are morphologically and physiologically identifiable and execute well-defined neuronal computations^{16–18}. One of the first computations described in RGCs is the computation of image motion¹⁹. Both ON and ON-OFF direction-selective ganglion cells (DSGCs) fire action potentials in response to visual stimuli moving across their receptive field in a particular (preferred) direction and are silenced when stimuli move in the opposite (null) direction^{19–23}. The neuronal circuitry underlying the computation of object motion has been studied intensively^{22,24–29}. The direction-selective action potential output of DSGCs is dependent on starburst amacrine cells (SBACs)^{25,30,31}, retinal interneurons that generate directionally tuned synaptic inhibition²⁴. It is, however, unknown how SBAC-mediated inhibition is integrated with light-evoked excitatory synaptic input to shape the direction-selective action potential output of DSGCs.

Notably, pioneering studies have found that direction-selective responses are evoked by light stimuli restricted to limited areas of the receptive field of DSGCs²⁰, suggesting that multiple dendritic integrative compartments, but not whole-cell integrative mechanisms, underlie the computation of image motion^{20,32}. One possibility is that such local integration arises through the engagement of active dendritic integration. Consistent with this, the generation of light-evoked dendritic spikes in DSGCs has been inferred by the silencing of axonal action potential output following the axo-somatic blockade of sodium channels³³. Although the role of active dendritic integration in the generation of directional selectivity has been highlighted in computation models³⁴, it has not been tested experimentally because of the difficulty of recording from the small-caliber dendrites of DSGCs ensheathed by glial-cell processes^{35,36}. We directly investigated the dendritic mechanisms underlying direction selectivity in rabbit DSGCs using dendritic and somatic electrophysiological recording techniques. We found that the activation and inhibitory synaptic control of a cascade of active dendritic integration compartments underlies this well-defined circuit-based computation.

RESULTS

Simultaneous whole-cell current-clamp recordings were made from the soma and the parent dendrites of ON-DSGCs, which exhibited directionally tuned patterns of axonal action potential firing in response to the movement of light bars across their receptive fields (direction index of action potential firing = 0.93 ± 0.01 ; 34 cells, 34 sections, 24 rabbits; **Fig. 1a–c**). Direct dendritic recordings revealed that light-evoked axonal action potentials were driven by dendritic spikes (**Fig. 1d–i**). When dendritic recordings were made from the area of the dendritic tree first activated by preferred-direction moving light bars, the preferred side of the dendritic tree, dendritic spikes with a complex rising phase preceded somatically recorded axonal

Queensland Brain Institute, The University of Queensland, Brisbane, Australia. Correspondence should be addressed to S.R.W. (srw@uq.edu.au).

Received 22 August; accepted 4 October; published online 27 October 2013; doi:10.1038/nn.3565

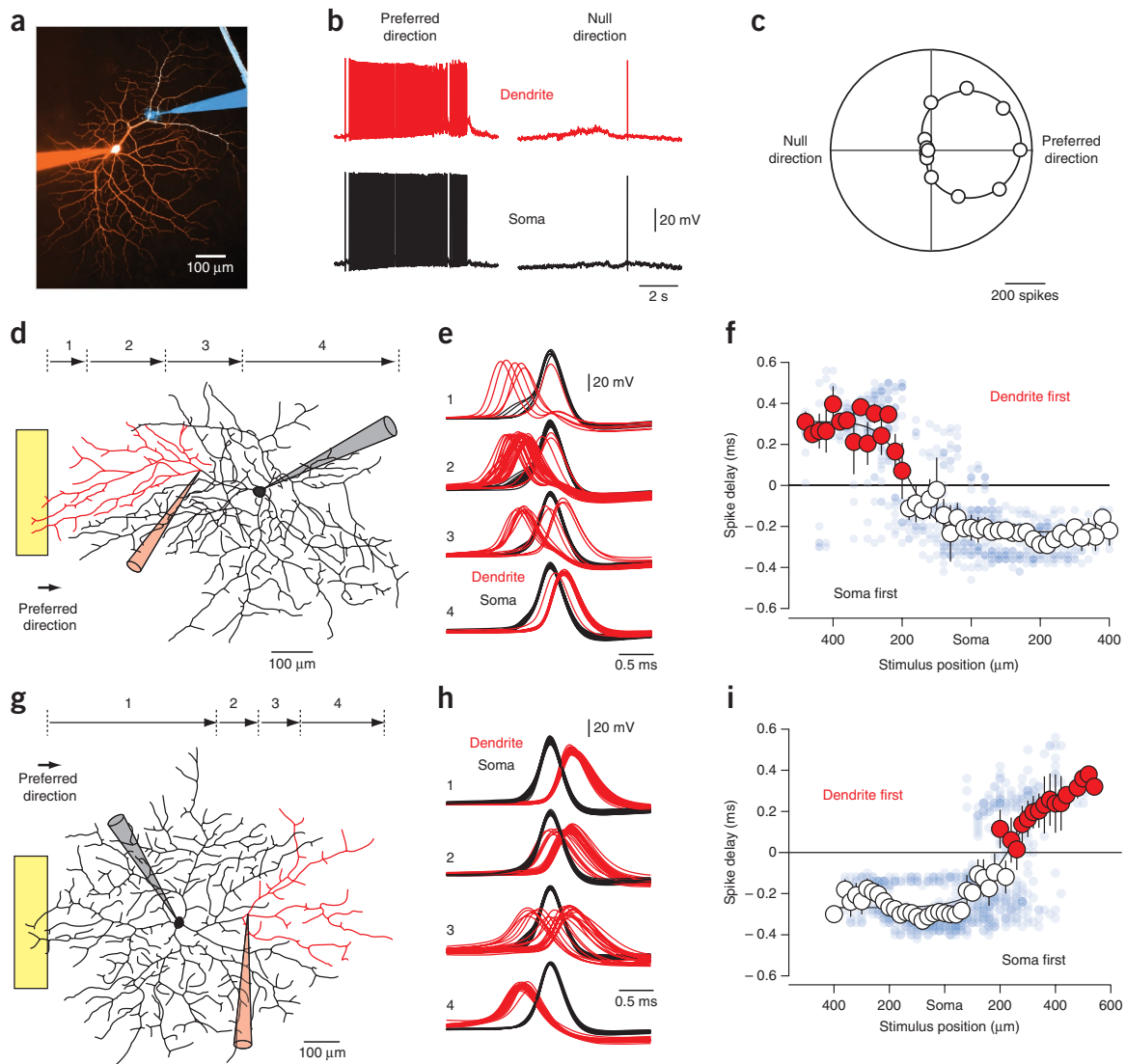


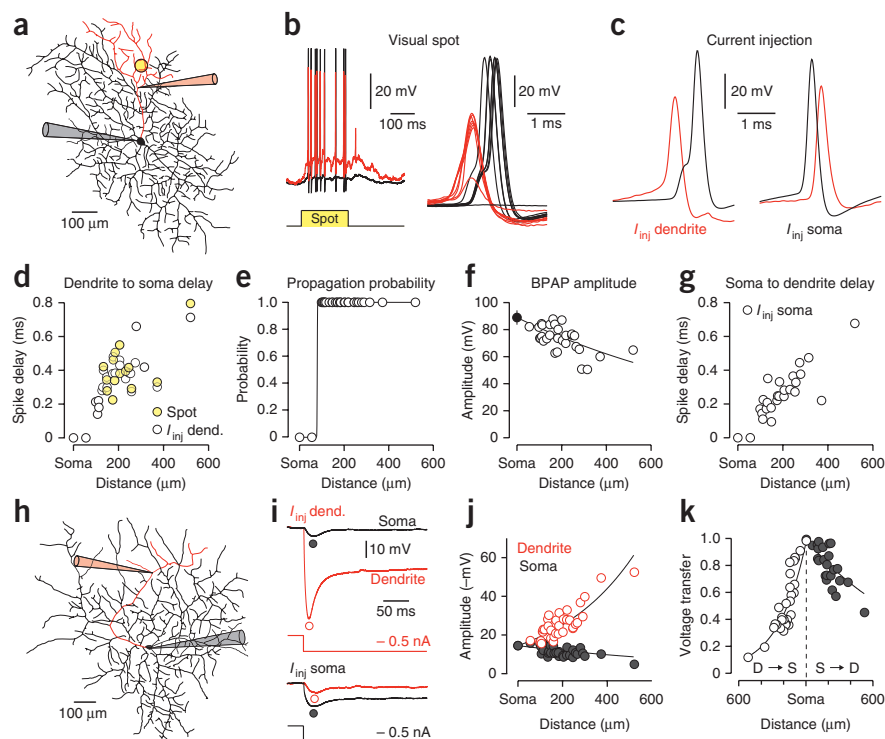
Figure 1 Dendritic spikes are evoked by visual stimuli. **(a)** Merged fluorescence photomicrograph of an ON-DSGC filled with Alexa Fluor 594 (orange, somatic recording) and Alexa Fluor 488 (blue, dendritic recording). **(b)** Somatic (black traces) and dendritic (red traces) recording of neuronal activity evoked by preferred- and null-direction moving light bars. **(c)** Polar plot of direction-selective action potential output (same cell shown in **b**, line represents a sine fit). **(d, g)** Schematic reconstructions of ON-DSGCs showing the placement of recording electrodes and the preferred-direction movement of a light bar. The red colored arbor indicates the recorded dendritic sub-tree. **(e)** Simultaneous somatic (black traces) and dendritic (red traces) recordings of dendritic spikes evoked when a preferred-direction light bar entered the preferred side of the dendritic tree (positions 1 and 2 in **d**) and the back-propagation of axonal action potentials when the light bar exited the null side (position 4 in **d**). In **e** and **h**, traces are aligned to the peak of somatically recorded action potentials. **(f)** Summary data of spike delay for seven cells (from seven rabbits) recorded dendritically from the preferred side (large symbols represent mean \pm s.e.m., small symbols represent individual data points). **(h)** Simultaneous somatic (black traces) and null-side dendritic recordings (red traces) of regenerative activity evoked by preferred-direction light stimuli. Dendritic spikes were initiated when the light stimulus traveled over the null side of the dendritic tree (positions 3 and 4 in **g**). **(i)** Summary data of spike delay for eight cells (eight sections, seven rabbits) recorded dendritically from the null side (large symbols represent mean \pm s.e.m., small symbols represent individual data points).

action potentials ($154 \pm 24 \mu\text{m}$ from the soma; 7 cells, from 7 rabbits; **Fig. 1d–f**). As the moving light bar swept past the dendritic recording electrode location and traveled toward the soma and into the contralateral, null side of the dendritic tree, evoked action potentials back-propagated to the dendritic recording site (**Fig. 1d–f**). We observed an inverse pattern of activation in response to preferred-direction light stimuli when dendritic recordings were made from the null side of the dendritic tree ($182 \pm 15 \mu\text{m}$ from the soma; 8 cells, 8 sections, 7 rabbits; **Fig. 1g–i**). Consequently, for recordings made from the preferred and null sides of the dendritic tree, light stimuli at sites distal to the recording electrode typically generated dendritic spikes that

preceded somatically recorded action potentials, whereas light stimuli at sites proximal to the dendritic recording electrode evoked activity first recorded from the soma (**Fig. 1f, i**). In contrast, in the same recordings, light bars moving in the null direction initiated almost no dendritic spikes and evoked sparse action potential firing (2 dendritic spikes, 52 action potentials; 15 cells, 15 sections, 14 rabbits).

To determine the factors controlling the electrical excitability of the dendritic tree of ON-DSGCs, we visually stimulated restricted areas of the receptive field with small flashing light spots, positioned close to the dendritic recording electrode (**Fig. 2**). These stimuli reliably generated dendritic spikes with a complex rising phase, which rapidly

Figure 2 Forward propagation of dendritic spikes. **(a)** Reconstruction of an ON-DSGC showing electrode placement and location of a flashing-spot stimulus (yellow circle). The red colored arbor indicates the recorded dendritic sub-tree. **(b)** Simultaneous somatic (black trace) and dendritic recording (red trace) of visually evoked activity (cell shown in **a**). Expanded traces show the variable amplitude and time course of dendritic spikes (red traces) and somatically recorded action potentials (black traces). Traces are aligned to the peak of dendritic spikes. **(c)** Direct dendritic (0.2 nA, left traces) or somatic (0.2 nA, right traces) current injection evoked dendritic spikes and back-propagating action potentials, respectively. **(d)** Distance-dependent increase in the time delay between current-evoked (open symbols) and light-evoked (yellow symbols) dendritic spikes and action potential firing (25 cells, 25 sections, 16 rabbits). **(e)** Dendritic spikes evoked by current injection >55 μm from the soma invariably trigger action potential output (31 cells, 31 sections, 24 rabbits). **(f)** Distance-dependent decrement in the amplitude of back-propagating action potentials (BPAPs, open symbols) evoked by somatic current injection (25 cells, 25 sections, 16 rabbits). The filled symbol indicates the average (\pm s.e.m.) amplitude of somatically recorded action potentials and the line represents an exponential fit to the data. **(g)** Distance-dependent delay in BPAPs invasion of the dendritic arbor (25 cells, 25 sections, 16 rabbits). **(h)** Reconstruction of an ON-DSGC showing electrode placement. The dendritic path between recording electrodes is shown in red. **(i)** Simultaneously recorded dendritic (red traces, 519 μm from the soma) and somatic (black traces) voltage responses evoked by negative current steps (-0.5 nA) delivered to the dendritic (upper traces) or somatic (lower traces) recording electrode (same cell shown in **h**). **(j)** Distance-dependent increase in the local amplitude of dendritic voltage responses (red symbols) and decrease in the amplitude of somatic responses (black symbols). **(k)** Asymmetric distance-dependent attenuation of subthreshold voltage responses, generated at dendritic (D-S) or somatic (S-D) sites. Lines in **j** and **k** represent exponential fits to the data (36 cells, 36 sections, 26 rabbits).



forward-propagated to the axon to drive neuronal output (25 cells, 25 sections, 16 rabbits; **Fig. 2b,d**). Furthermore, direct excitation of parent dendrites by the injection of positive current steps through the recording electrode generated dendritic spikes, which invariably drove action potential firing in recordings made >55 μm from the soma (31 cells, 31 sections, 24 rabbits; **Fig. 2c-e**). In contrast, the injection of positive current steps at proximal dendritic or somatic recording sites evoked axonal action potentials, which rapidly back-propagated to dendritic recording sites with little amplitude decrement (**Fig. 2c,f,g**).

The direct observation of light-evoked dendritic spike generation in DSGCs demonstrates, to the best of our knowledge for the first time, the active dendritic integration of sensory input in the CNS, extending previous findings detailing the active dendritic integration of synaptic input in the electrically distributed dendritic trees of other classes of central neuron³⁻¹¹. To explore the factors that shape active dendritic integration in DSGCs, we first examined the underlying electrotonic structure of these cells by recording the distance-dependent attenuation of subthreshold voltage responses as they spread through the dendritic tree (36 cells, 36 sections, 26 rabbits; **Fig. 2h-k**). At the dendritic site of generation, the amplitude of subthreshold voltage responses evoked by negative current steps markedly increased as parent dendritic recordings were made from increasingly remote sites (**Fig. 2h,i** and **Supplementary Fig. 1**). The amplitude of dendritically generated subthreshold voltage responses, however, attenuated as they spread to the soma, revealing pronounced distance-dependent dendro-somatic voltage attenuation (voltage transfer = $V_{\text{soma}}/V_{\text{dendrite}}$; **Fig. 2k**). In contrast, the somato-dendritic attenuation of subthreshold voltage responses was far less

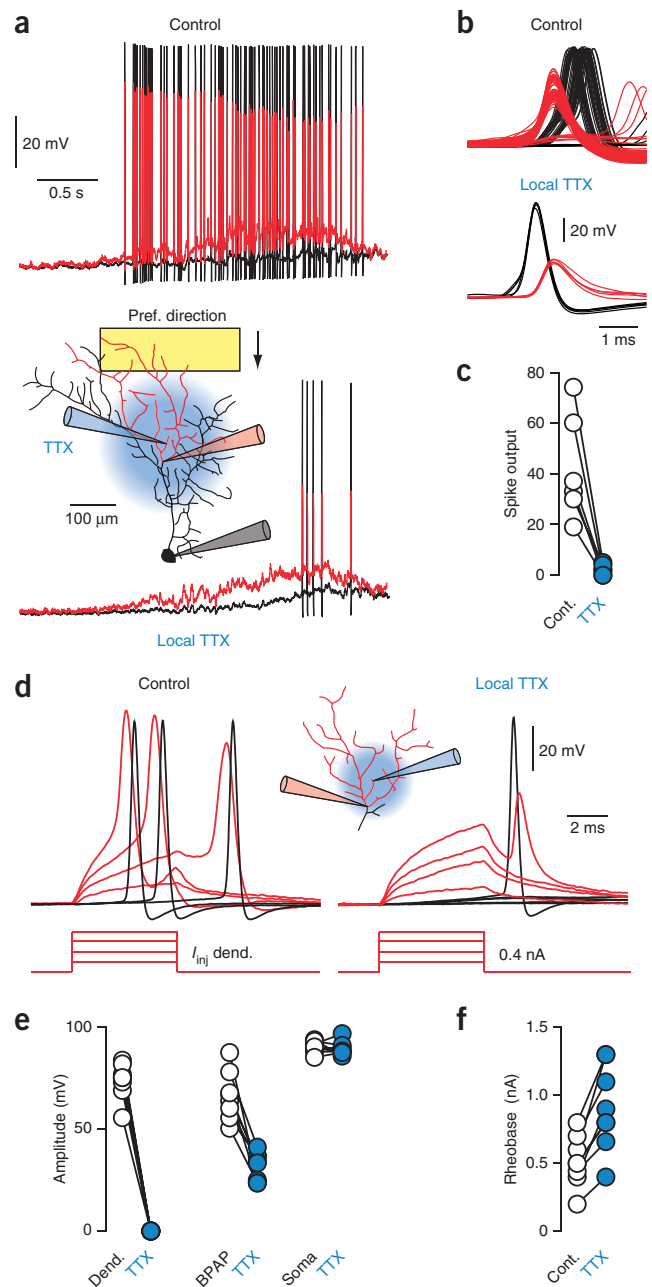
severe (voltage transfer = $V_{\text{dendrite}}/V_{\text{soma}}$; **Fig. 2k**), consistent with results from neuronal models³⁷. These data indicate that the dendritic arbor of DSGCs is electrically distributed and highlight the necessity for dendritic spike generation to drive action potential firing as light stimuli enter and move across the wide receptive fields of DSGCs.

We next examined the properties of the voltage-activated ion channels that support active dendritic integration in DSGCs. The brief duration of dendritic spikes suggests that these events are mediated by the regenerative recruitment of voltage-activated sodium channels^{9,11,38}. To test this, we locally applied the sodium channel blocker tetrodotoxin (TTX, 1–10 μM) to an area of the dendritic tree close to the recording electrode (**Fig. 3a-c**). Local dendritic TTX application significantly reduced the action potential output of ON-DSGCs evoked by preferred-direction moving light bars as they passed over the recorded dendritic tree by blocking dendritic spike initiation (6 cells from 6 rabbits, $P = 0.002$; **Fig. 3b,c**). Similarly, local dendritic TTX application prevented the direct initiation of dendritic spikes by steps of positive current delivered through the recording electrode, and so increased the dendritic excitatory input required to drive action potential firing (8 cells from 8 rabbits, $P < 0.001$; **Fig. 3d-f**). Inversely, the local application of TTX to the soma selectively reduced light-evoked axonal action potentials, but did not disturb dendritic spike generation (**Supplementary Fig. 2**). Although dendritic TTX application did not alter the somatic amplitude of action potentials ($P = 0.5862$), it markedly reduced their amplitude as they spread to the dendritic recording site, indicating that dendritic sodium channels underlie the active back-propagation of action potentials³⁹ in DSGCs ($P < 0.001$; **Fig. 3d,e**).

Figure 3 Dendritic spikes amplify sensory input. **(a)** Local dendritic application of TTX reduces preferred-direction light-evoked action potential output. Simultaneous dendritic (red traces) and somatic recordings (black traces) are shown under control conditions (upper traces) and during TTX application (lower traces). The inset shows the placement of electrodes, the application site of TTX (1 μ M, blue) and schematic light bar movement (yellow rectangle). **(b)** Expanded traces show dendritic spike generation under control conditions (dendrite red, soma black upper traces) and sparse back-spread of action potentials following dendritic TTX application. **(c)** Summary of the reduction of moving light bar-evoked action potential output by local dendritic TTX ($P = 0.002$, 6 cells from 6 rabbits, paired Student's t test). **(d)** Dendritic input-output relationship evoked by direct current injection under control and during local dendritic TTX application. The inset shows the recording configuration. **(e)** Local dendritic TTX reduced the peak amplitude of directly evoked dendritic spikes (Dend., $P < 0.001$) and BPAPs ($P < 0.001$), but not that of somatically recorded action potentials (soma, $P = 0.5862$) (paired Student's t test). **(f)** Threshold dendritic current (rheobase) for generating action potential output under control and during local dendritic TTX application ($P < 0.001$) (paired Student's t test). $n = 8$ cells from 8 rabbits **(e,f)**.

A notable morphological feature of the dendritic tree of DSGCs is their lattice-like structure, with parent dendrites giving rise to multiple thin space-filling terminal dendrites^{23,36}. Ultrastructural studies have shown that the excitatory glutamatergic synapses from bipolar cells, which mediate light-evoked excitation of DSGCs, are concentrated on terminal dendrites^{40,41}. To determine whether we could detect the electrical signature of active dendritic integration in terminal dendrites, which are not permissive to direct recording, we analyzed the amplitude distribution and time course of dendritic spikes recorded from parent dendrites in response to preferred-direction moving light bars. In each recording, we observed large- and small-amplitude light-evoked dendritic spikes (Fig. 4a). Pooled data revealed that the amplitude distribution of light-evoked dendritic spikes was bimodal ($206 \pm 18 \mu$ m from the soma, 21 cells from 21 rabbits; Fig. 4b). Simultaneous somatic recordings showed that the predominant large-amplitude dendritic spikes reliably drove axonal action potential output (probability = 0.997, $n = 5,870$ spikes; Fig. 4c), whereas the less common small-amplitude spikes strongly attenuated as they spread to the soma, producing voltage waveforms that were often barely detectable ($n = 1,122$ spikes; Fig. 4d and Supplementary Fig. 3). Given that both small- and large-amplitude dendritic spikes were evoked during a visual response, we reasoned that small-amplitude dendritic spikes might be generated at terminal dendritic sites and act as triggers for the generation of large-amplitude spikes in the parent dendrite.

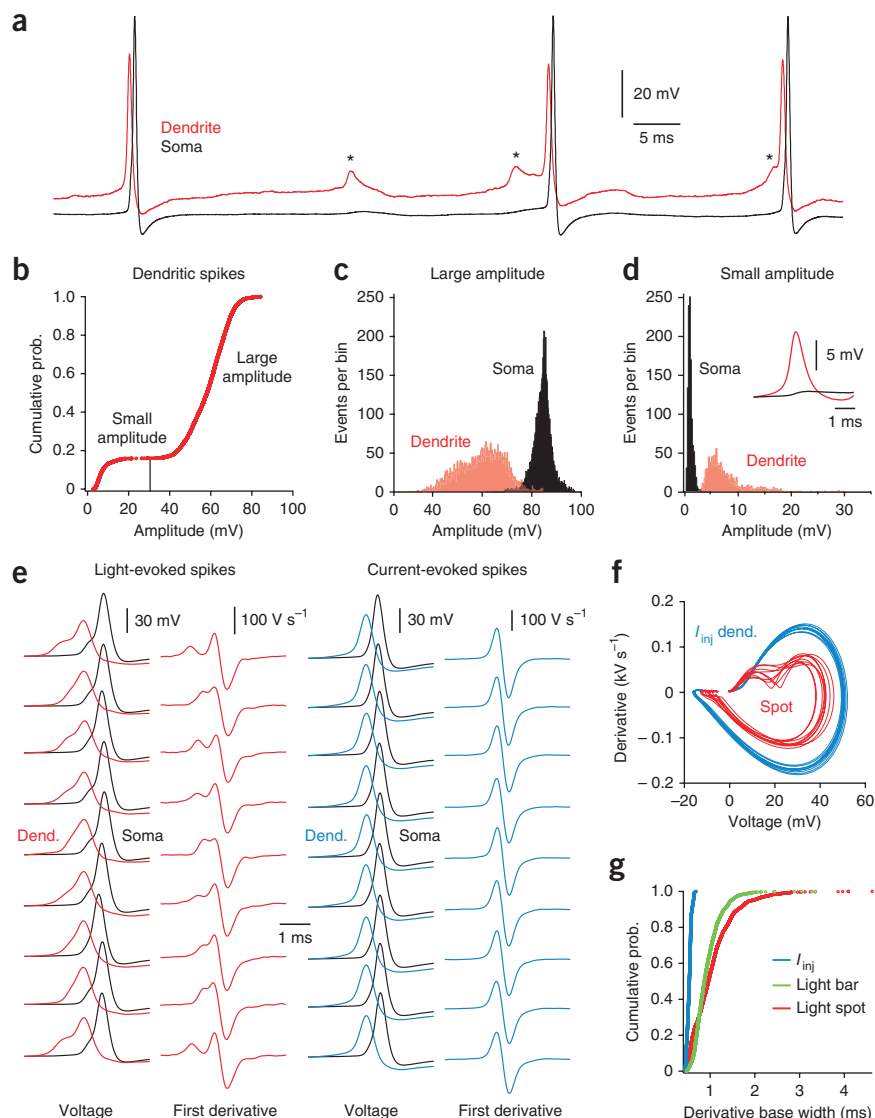
To examine this possibility, we analyzed the rising phase of large-amplitude dendritic spikes evoked by flashing spot and preferred-direction moving light stimuli. Light-evoked large-amplitude dendritic spikes characteristically possessed a complex, dual-component rising phase (Fig. 4a,e). The separation of these components was more evident when we calculated the first derivative of dendritic spikes, with the first derivative of individual large-amplitude dendritic spikes exhibiting a dual-component positive peak (Fig. 4e). In contrast, in the same recordings, dendritic spikes evoked by direct current injection had a simple mono-phase rise with single-positive peaked first derivatives (Fig. 4e), a difference that was evident in phase plots (Fig. 4f). Pooled data revealed that the time course of the rising phase of the first derivative of light-evoked large-amplitude dendritic spikes was substantially longer than those generated by direct current injection (Fig. 4g). Thus, the dual-component nature of light-evoked large-amplitude dendritic spikes suggests that small-amplitude (terminal dendritic) spikes precede and act as triggers for parent dendritic spike generation. Consistent with



this interpretation, simulations revealed that the dual-component rising phase of light-evoked large-amplitude dendritic spikes could be reproduced by the addition, with variable delays, of experimentally recorded small-amplitude terminal dendritic spikes and current-evoked parent dendritic spikes (Supplementary Fig. 4).

To critically examine the electrical excitability of terminal dendrites, we examined whether small-amplitude dendritic spikes could be evoked in isolation when light stimuli selectively excited terminal dendritic sites (Fig. 5). When we presented flashing light stimuli to small areas of the receptive field that corresponded to both parent and terminal dendritic sites, both small- and large-amplitude dendritic spikes were generated (Fig. 5a). In contrast, when the diameter of the light spot was decreased and selectively overlaid terminal dendritic sites, small-amplitude dendritic spikes were generated in isolation (Fig. 5a,c). The local application of TTX to terminal dendritic sites

Figure 4 Properties of dendritic spikes in DSGCs. **(a)** Generation of small- (*) and large-amplitude dendritic spikes (red trace) recorded 200 μm from the soma (black trace) in response to preferred-direction moving light bar. **(b)** Bimodal amplitude distribution of dendritic spikes generated in response to preferred-direction moving light bars (7,007 dendritic spikes from 21 cells, 21 sections, 21 rabbits). The distribution can be divided into small-amplitude dendritic spikes (<30 mV) and large-amplitude dendritic spikes (>30 mV). **(c)** Amplitude distribution of light-evoked large-amplitude dendritic spikes (>30 mV amplitude) at dendritic (red bars) and somatic (black bars) recording sites. Note that 5,870 of 5,885 large-amplitude dendritic spikes drove action potentials. **(d)** Amplitude distribution of small-amplitude dendritic spikes (<30 mV amplitude, red bars) revealed their weak direct somatic effect (black bars). The inset shows the average of ten small-amplitude dendritic spikes (red trace) recorded 200 μm from the soma. **(e)** Light stimuli evoked dual-component dendritic spikes (left traces), whereas current stimuli evoked single-component dendritic spikes (right traces). **(f)** Phase plots of the light- and current-evoked dendritic spikes shown in **e**. **(g)** Time course of the rising phase of large-amplitude dendritic spikes evoked by light stimuli (spot and moving bar) and dendritic current (I_{inj}). Time course was measured at 5% of the positive peak of the first derivative (light spots: dendritic recordings $221 \pm 26 \mu\text{m}$ from the soma, $n = 3,072$ dendritic spikes; moving light bars: dendritic recordings $206 \pm 87 \mu\text{m}$ from the soma, $n = 3,099$ dendritic spikes; 21 cells, 21 sections, 21 rabbits).



co-aligned with terminal dendritic flashing light stimuli reversibly abolished the initiation of isolated small-amplitude spikes, confirming that they represent regenerative terminal dendritic spikes (6 cells from 6 rabbits, $P < 0.001$;

Fig. 5b–g). Terminal dendritic TTX application, however, did not alter the underlying subthreshold visually evoked synaptic activity²² ($P = 0.4811$) or the amplitude of current-evoked parent dendritic spikes ($P = 0.1358$) and axonal action potentials ($P = 0.8813$; **Fig. 5e–g**). Taken together, these data indicate that light-evoked excitatory synaptic input activates a cascade of active integration compartments in the dendritic tree of ON-DSGCs. Spikes are first initiated at terminal dendritic sites and subsequently recruit parent dendritic integration compartments to form dendritic spikes with a complex waveform, which reliably propagate to the axon to initiate neuronal output.

This scheme suggests that the inhibitory synaptic control of direction selectivity in DSGCs^{23,24,27} may be mediated by the control of active dendritic integration. To test this, we first pharmacologically reduced synaptic inhibition by applying a GABA_A-receptor antagonist to the entire retinal circuit (**Fig. 6a**). Somatic recording revealed that the blockade of GABA_A receptors abolished the direction selectivity of action potential output (direction index, control = 0.93 ± 0.04 , GABA_A (SR-95531, 10 μM) = 0.07 ± 0.08 , 6 cells from 6 rabbits; **Fig. 6a**). Simultaneous dendritic recording revealed that GABA_A receptor blockade transformed the pattern of dendritic activity elicited by null-direction light stimuli, replacing the sparse pattern of action potential

back-propagation with both terminal (small amplitude) and parent (large amplitude) dendritic spike generation (6 cells from 6 rabbits; **Fig. 6b,c**). Thus, the blockade of synaptic inhibition unmasks dendritic spike initiation in response to null-direction visual stimuli.

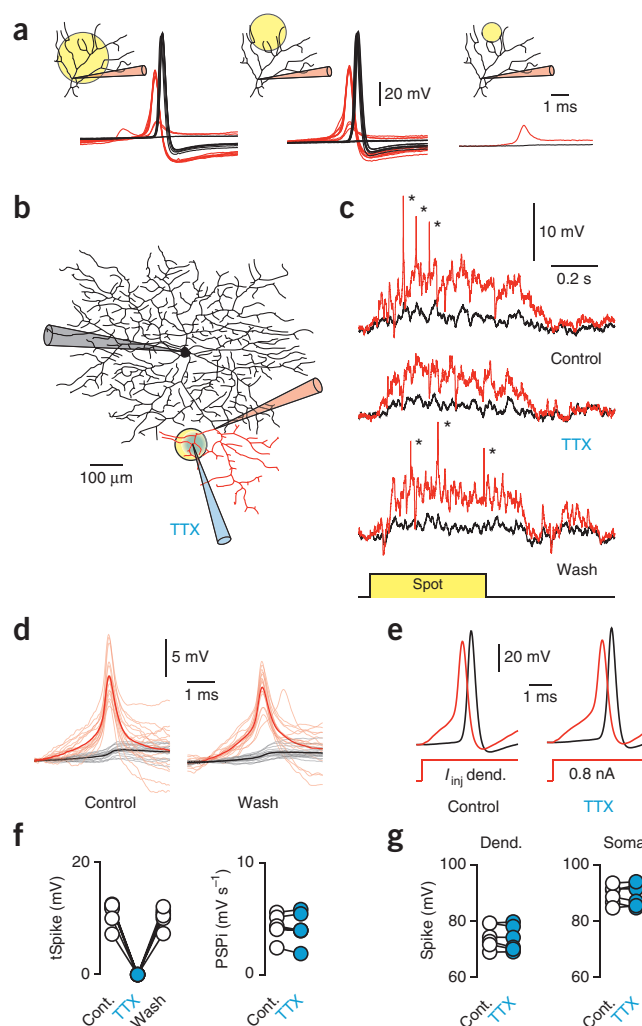
Where does synaptic inhibition exert its actions in the active integration cascade? To answer this question, we first explored the inhibitory synaptic control of parent dendritic excitability. Simultaneous somatic and parent dendritic recordings revealed that null-direction light-evoked postsynaptic inhibition was greatest in amplitude at dendritic recording sites (**Supplementary Fig. 5**). Consequently, we examined the effect of null-direction light-evoked synaptic inhibition on direct current-evoked parent dendritic spike initiation by the construction of input-output relationship under control conditions and during light-evoked synaptic inhibition (**Fig. 7** and Online Methods). Notably, the slow small-amplitude envelope of depolarization decorated by inhibitory postsynaptic potentials (IPSPs) evoked by null-direction moving light bars (**Figs. 1b** and **7c**)²² decreased the threshold current for the initiation of parent dendritic spikes (control rheobase = 0.97 ± 0.13 nA, null-direction rheobase = 0.71 ± 0.13 nA, 5 cells from 5 rabbits, $P = 0.0037$; **Fig. 7b**) and did not hamper the forward-propagation of parent dendritic spikes (control propagation

Figure 5 Cascade of active dendritic integration compartments in DSGCs. (a) Isolated small-amplitude dendritic spikes were evoked when a flashing light spot (yellow circles) was restricted to a small terminal region of the dendritic field. (b) Reconstruction of an ON-DSGC showing the placement of electrodes and the coincident location of a small flashing light spot (yellow circle) and the area of tetrodotoxin application (TTX, 1 μ M, blue). (c) Light spot-evoked small-amplitude dendritic spikes (red traces, *) were reversibly blocked by local terminal dendritic TTX application. (d) The waveform of small-amplitude dendritic spikes recorded at the parent dendrite (red traces, 245 μ m from the soma) and the soma (black traces) under control and following washout of TTX (solid traces are averages of 17 spikes). (e) Current-evoked parent dendritic spikes were unaffected by terminal dendritic TTX application. Traces in c–e were recorded from the ON-DSGC illustrated in b. (f) Small-amplitude dendritic spikes were abolished by local TTX application (tSpike, $P < 0.001$), but local TTX did not alter the area of light-evoked synaptic activity (PSPi = integral of the postsynaptic response, $P = 0.4811$) (paired Student's t test). (g) Terminal dendritic TTX did not alter the amplitude of current-evoked parent dendritic spikes (dend., $P = 0.1358$) and somatic action potentials (soma, $P = 0.8813$) (paired Student's t test). $n = 6$ cells from 6 rabbits (f,g).

probability = 1, null-direction propagation probability = 1, 8 cells from 8 rabbits), but did increase the temporal jitter between parent dendritic spike generation and action potential initiation (spike jitter: control = 0.047 ± 0.02 ms, null-direction inhibition = 0.20 ± 0.07 ms; dendritic current step: duration = 2 ms, amplitude = 0.88 ± 0.07 nA; Fig. 7c). The inability of light-evoked synaptic inhibition to control parent dendritic spike generation suggests that synaptic inhibition may act at the level of terminal dendrites. To test this, we locally applied the GABA_A receptor antagonist to small regions of terminal dendrites (Fig. 7d). The local terminal dendritic antagonism of GABA_A receptors unmasked terminal and parent dendritic spike generation in response to null-direction light bars as they passed over the affected terminal dendrites (5 cells from 5 rabbits; Fig. 7d–g). Pooled data revealed that the localized dendritic blockade of GABA_A receptors revealed null-direction light-evoked dendritic regenerative activity with a structure that was indistinguishable from that generated by preferred-direction stimuli under control conditions (Figs. 4b and 7g). Inhibitory synaptic control of terminal dendritic active integration is therefore the cornerstone of the computation of direction selectivity in ON-DSGCs.

DISCUSSION

Direct electrical recording and imaging approaches have revolutionized our understanding of central neurons, revealing the active integration of dendritic synaptic input at the level of single dendritic

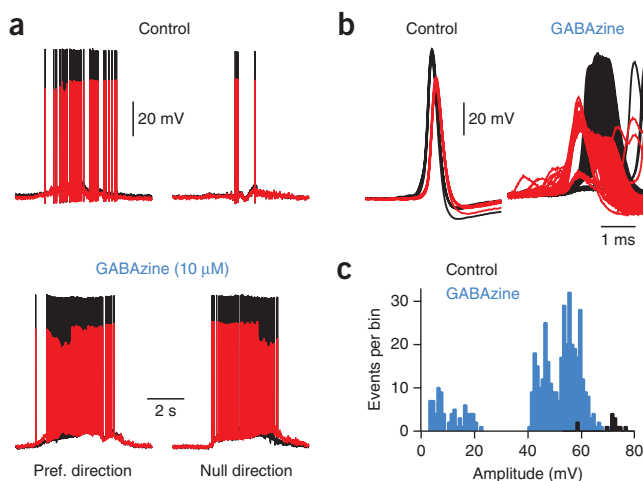


branches and trees^{3–9,11,38}. Evidence for the engagement of active dendritic integration by physiological stimuli and its role in neuronal computation is, however, limited, as a result of the technical difficulty of applying direct recording approaches^{14,33,42,43}. To directly address this issue, we combined multi-site somatic and dendritic electrical recording techniques with the maintenance of an intact and functional neuronal circuit *in vitro* to demonstrate that active dendritic integration underlies the computation of direction selectivity in the output neurons of the retina.

Active dendritic integration in DSGCs

The architecture of the retinal neuronal network is well described. High-resolution anatomical techniques have mapped the retinal

Figure 6 Null-direction light-evoked inhibitory synaptic control of dendritic integration. (a) Antagonism of GABA_A receptors abolished direction selectivity. Simultaneous somatic (black) and dendritic (red, 111 μ m from soma) recordings of preferred- and null-direction light responses under control conditions and during bath application of the GABA_A receptor antagonist GABAzine (10 μ M) are shown. (b) Blockade of GABA_A receptors unmasked dendritic electrogenesis evoked by null-direction light stimuli. (c) Amplitude distribution of null-direction light evoked terminal and parent dendritic spikes when GABA_A receptors were antagonized (blue bars). The black bars show the amplitude distribution of back-propagating action potentials under control conditions (6 cells from 6 rabbits).



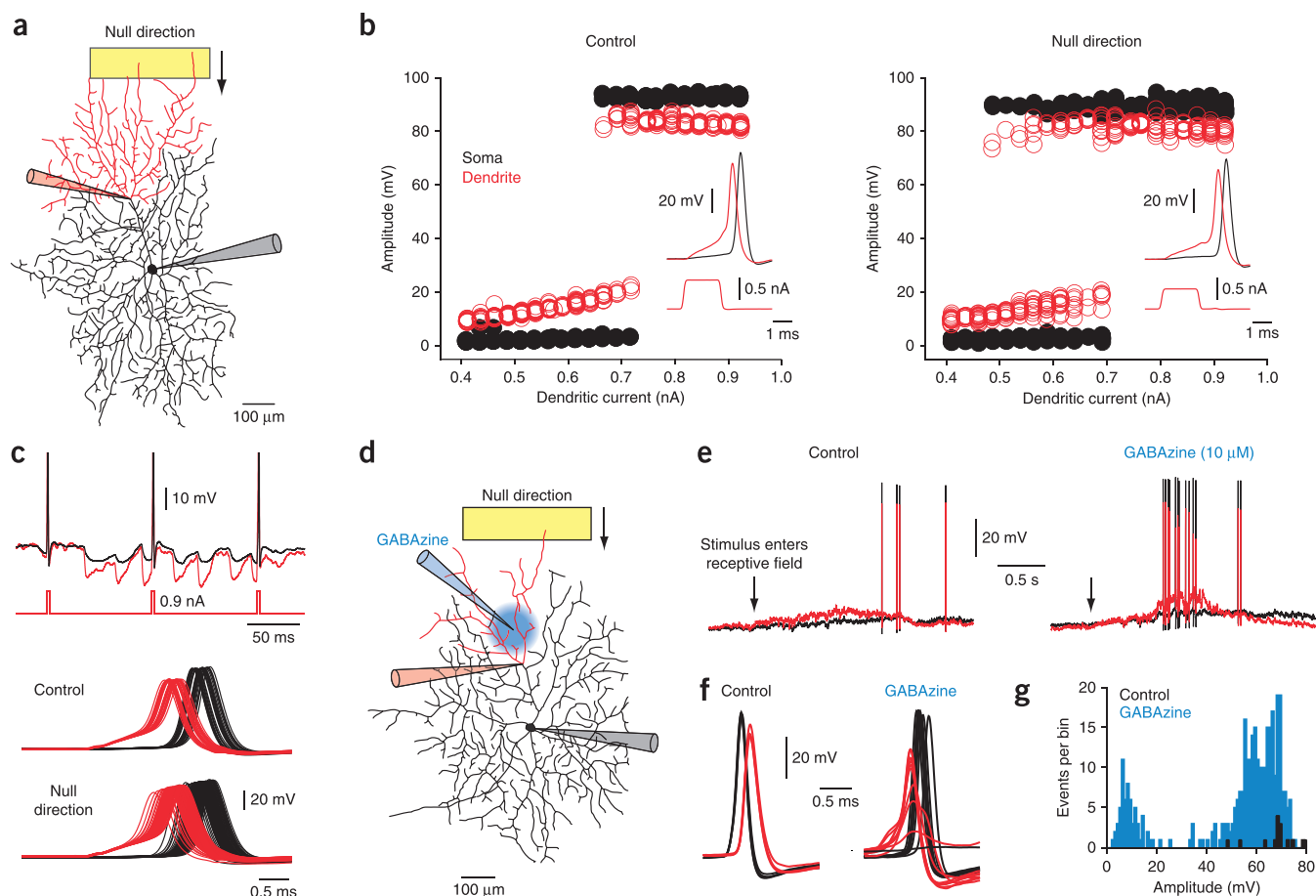


Figure 7 Inhibitory synaptic control of terminal dendritic integration underlies direction selectivity. **(a)** Reconstruction of an ON-DSGC showing the placement of electrodes and the schematic null-direction movement of a light bar. **(b)** Dendritic input-output relationship in the absence (left) and presence of null-direction light stimuli (right). Note that null-direction light stimuli decreased the rheobase current for parent dendritic spike initiation. Insets, rheobase current-evoked dendritic spikes from the DSGC in **a**. **(c)** Null-direction light-evoked inhibitory postsynaptic potentials did not block the initiation or forward propagation of directly generated parent dendritic spikes, but did increase their temporal jitter (red traces, 264 μm from the soma). **(d)** Reconstruction of an ON-DSGC showing the placement of electrodes, the schematic null-direction movement of a light bar and the area of local terminal dendritic GABAzine (10 μM , blue) application. **(e, f)** Terminal dendritic application of GABAzine unmasked dendritic electrogenesis evoked by null-direction light stimuli. Simultaneous dendritic (red traces, 183 μm from the soma) and somatic recordings showed sparse null-direction light-evoked action potential back-propagation under control conditions and terminal and parent dendritic spiking that drove action potential output following terminal dendritic GABAzine application. **(g)** Bimodal amplitude distribution of dendritic spikes evoked by null-direction light bars following terminal dendritic GABAzine application (blue bars, 5 cells from 5 rabbits). The black bars show the amplitude distribution of back-propagating action potentials evoked under control conditions.

circuitry underlying direction selectivity^{27,31}, together with the sub-cellular position of excitatory and inhibitory synaptic contacts in the dendritic arbor of DSGCs⁴¹. Despite this, a mechanistic description of the integrative operations underlying the direction-selective action potential output of DSGCs has not emerged, partly as a result of the difficulty of making direct electrical recording from small-caliber dendrites ensheathed by glial-cell processes^{35,36}. Direct electrical recordings have been made from the dendrites of large RGCs following enzymatic disassociation from glial-cell processes, a procedure which precludes the study of the dendritic integrative mechanisms engaged by light stimuli³⁵. Recordings from enzymatically dissociated RGCs have shown that action potentials spread decrementally into the dendritic tree and that small-amplitude dendritic spikes can be generated by direct current injection, which spread to the soma in a decremental manner leading to somatically recorded spikelets that intermittently precede axonal action potential firing³⁵. Consistent with this, the silencing or weakening of axonal action potential initiation

by the peri-somatic application of TTX has revealed the presence of preferred-direction light-evoked somatically recorded spikelets in DSGCs in the intact retinal network³³. Furthermore, two-photon calcium imaging has demonstrated that the local dendritic application of TTX decreases light-evoked dendritic calcium signaling, although it is unclear whether this effect is mediated by a reduction of active dendritic integration or a reduction of the dendritic back-spread of axonal action potentials³³.

We took advantage of the relatively simple dendritic arbor of sustained ON-DSGCs, which possess a single radial dendritic tree confined to sublamina-B of the inner plexiform layer²³ readily accessible to recording electrodes, and found that sodium channel-dependent dendritic spikes were generated in response to preferred-direction moving light bars, spatially restricted light spots and direct current injection. Light-evoked parent dendritic spikes forward-propagated to the axon to initiate action potential firing with a high probability (0.9971). Dendritic spike initiation and active forward propagation

therefore overcomes the intense distance-dependent dendro-somatic electrical filtering properties of the dendritic arbor of DSGCs to ensure the efficient driving of neuronal output by light-evoked excitatory synaptic input. We build on these findings to dissect a multi-layered active dendritic integration scheme for DSGCs.

Direct dendritic recording revealed that active dendritic integration in DSGCs is a multi-layered process. Light-evoked dendritic spikes, but not current-evoked dendritic spikes, were characterized by a dual-component rise. We suggest that the dual-component rise of light-evoked dendritic spikes arises from dendritic spike generation in terminal dendrites, the predominant site of excitatory synaptic input to DSGCs⁴¹, which, in turn, trigger parent dendritic spike initiation. Consistent with this, parent dendritic recordings revealed that small- and multi-phasic large-amplitude dendritic spikes were generated in response to preferred-direction light bars, that flashing spot light stimuli restricted to terminal dendritic sites evoked isolated small-amplitude dendritic spikes and that the local application of TTX to terminal dendrites blocked small-amplitude dendritic spike generation. Direct dendritic recordings therefore indicate that preferred-direction light stimuli activate a cascade of active dendritic integration compartments, initiated by local dendritic spike generation in terminal dendrites as branch-specific output responses, which in turn generate parent dendritic spikes as dendritic sub-tree output responses. Our findings reveal that the coupling between these integration compartments is secure, with less than a 20% rate of failure. The observation of isolated terminal dendritic spikes when light stimuli are restricted to terminal dendritic sites suggests that the coupling between integration compartments is enhanced during wide-field light stimulation as a result of the summation of terminal dendritic spikes with synaptic depolarization; in contrast, we rarely observed instances in which parent dendritic spikes were preceded by a summated series of terminal dendritic spikes. The decremental forward spread of terminal dendritic spikes to the parent dendrite is compatible with the morphology of DSGCs, where thin untapering terminal dendrites feed into larger diameter parent dendrites, creating an impedance mismatch that hampers their forward spread^{10,36}.

In direct support of this multi-layered active integration scheme, the local and selective dendritic application of TTX inhibited both terminal and parent dendritic spike generation and, as a consequence, greatly reduced the action potential output evoked by preferred-direction moving light bars, extending indirect findings recorded from the soma of ON-OFF DSGCs³³. Our integration scheme, however, is distinct from those previously inferred by somatic recording and computational modeling of DSGCs^{33,34} because of the multi-layered nature of active dendritic integration, which we found to be integral to both action potential generation as light stimuli entered and moved across the receptive field in a preferred direction and for the inhibitory synaptic control of neuronal output when light stimuli moved in the null direction.

Comparison with other central neurons

Our multi-layered active integration scheme has parallels with experimental and computational model findings from other central neurons^{7,10–13}. In cortical pyramidal neurons, the recruitment of voltage-activated channels and nonlinear excitatory synaptic mechanisms have been shown to generate dendritic spikes in multiple compartments^{6,7,9–11}. Two-photon glutamate uncaging techniques have revealed that the number of excitatory inputs required to generate dendritic spikes is lowest at terminal dendritic sites¹¹ and that the recruitment nonlinear mechanisms is greatest⁸ because of the high apparent input impedance. Our recordings revealed that the apparent

input resistance of DSGCs was not uniform and increased approximately fivefold at remote parent dendritic sites. If this increase extends to the terminal dendrites, as indicated by modeling studies^{34,44}, these findings suggest that excitatory synaptic input will generate large-amplitude local voltage responses at terminal dendritic sites, providing a substrate for the recruitment of terminal dendritic voltage-activated sodium channels.

Sodium channel-dependent spikes can be generated in multiple dendritic compartments of CA1 pyramidal neurons^{6,9,11}. The signaling role of dendritic sodium spikes is, however, limited in pyramidal neurons because of use- and frequency-dependent channel inactivation and rendered refractory for long time periods by action potential firing⁹. In comparison, we found that sodium channel-dependent dendritic spikes were generated at a high frequency in DSGCs and, despite the robust back-propagation of action potentials, axonal action potential firing inhibited dendritic spike generation for only ~2 ms (**Supplementary Fig. 6**). Thus, the properties of sodium channels in DSGCs allow dynamic high-frequency active dendritic integration.

Synaptic inhibition controls active dendritic integration

The computation of direction selectivity crucially involves the inhibition of DSGC action potential firing when light stimuli move across the receptive field in a null direction, a process mediated by dendritic GABA release from SBACs^{23,24,27}. High-resolution ultrastructural techniques have shown that SBACs make dendro-dendritic synaptic contacts with DSGCs, but do not directly innervate bipolar cell terminals^{27,31,40,45}, which are not directionally tuned⁴⁶. We found that both the global and local terminal dendritic pharmacological antagonism of GABA_A receptors transforms the output response of DSGCs, unmasking null-direction light-evoked terminal and parent dendritic spike generation with properties identical to those evoked by preferred-direction light stimuli. We therefore suggest that null-direction light-evoked IPSPs act to control the initiation of terminal dendritic spikes in DSGCs, thereby inhibiting the first stage of a multi-layered active integration cascade (**Supplementary Fig. 7**), a mechanism of inhibitory control that is distinct from that previously suggested by experimental and computation modeling approaches^{33,34}. In contrast with previous suggestions³³, we found that null-direction synaptic inhibition did not impede the forward propagation of parent dendritic spikes to the axon, an observation compatible with recent theoretical and experimental findings made from other central neurons that emphasize that distal dendritic synaptic inhibition is more effective at controlling dendritic nonlinearities than ‘on-path’ proximal dendritic inhibition^{47–49}. Consistent with this, we found that dendro-somatic voltage attenuation of null-direction light-evoked IPSPs in DSGCs was severe (**Supplementary Fig. 5**), suggesting that dendritic inhibitory synaptic conductance will be highly spatially compartmentalized⁵⁰. Dendritic synaptic inhibition is therefore unlikely to have widespread control of neuronal excitability, but will be most efficacious when positioned at sites close to bipolar cell excitatory inputs.

The multi-layered active dendritic integration scheme that we propose for DSGCs describes how excitatory and inhibitory synaptic inputs are integrated to control neuronal output during the computation of direction selectivity (**Supplementary Fig. 7**) and provides a mechanistic substrate for the implementation of direction-selective ‘subunits’ in the dendritic tree of DSGCs²⁰. Thus, our work complements the elegant description of the wiring of the retinal circuitry underlying direction selectivity²⁷ and directly suggests that the physiological activation and inhibitory synaptic control of active dendritic integration compartments underlie a fundamental neuronal computation.

METHODS

Methods and any associated references are available in the [online version of the paper](#).

Note: Any Supplementary Information and Source Data files are available in the [online version of the paper](#).

ACKNOWLEDGMENTS

We are grateful to D. Vaney, W. Taylor, W. Levick, M. Harnett, R. Tweedale and G. Murphy for critically reading the manuscript. This work was supported by grants from the Australian Research Council (FT100100502 and DP130101630) and National Health and Medical Research Council (APP1004575) to S.R.W. and a University of Queensland Early Career Researcher Award (2012003384) to B.S.

AUTHOR CONTRIBUTIONS

B.S. and S.R.W. conceived the project, designed the experiments and wrote the paper. B.S. conducted the experiments.

COMPETING FINANCIAL INTERESTS

The authors declare no competing financial interests.

Reprints and permissions information is available online at <http://www.nature.com/reprints/index.html>.

- Häusser, M., Spruston, N. & Stuart, G.J. Diversity and dynamics of dendritic signaling. *Science* **290**, 739–744 (2000).
- Johnston, D. & Narayanan, R. Active dendrites: colorful wings of the mysterious butterflies. *Trends Neurosci.* **31**, 309–316 (2008).
- Larkum, M.E., Zhu, J.J. & Sakmann, B. A new cellular mechanism for coupling inputs arriving at different cortical layers. *Nature* **398**, 338–341 (1999).
- Schiller, J., Major, G., Koester, H.J. & Schiller, Y. NMDA spikes in basal dendrites of cortical pyramidal neurons. *Nature* **404**, 285–289 (2000).
- Williams, S.R. & Stuart, G.J. Dependence of EPSP efficacy on synapse location in neocortical pyramidal neurons. *Science* **295**, 1907–1910 (2002).
- Ariav, G., Polsky, A. & Schiller, J. Submillisecond precision of the input-output transformation function mediated by fast sodium dendritic spikes in basal dendrites of CA1 pyramidal neurons. *J. Neurosci.* **23**, 7750–7758 (2003).
- Larkum, M.E., Nevian, T., Sandler, M., Polsky, A. & Schiller, J. Synaptic integration in tuft dendrites of layer 5 pyramidal neurons: a new unifying principle. *Science* **325**, 756–760 (2009).
- Branco, T., Clark, B.A. & Häusser, M. Dendritic discrimination of temporal input sequences in cortical neurons. *Science* **329**, 1671–1675 (2010).
- Remy, S., Csicsvari, J. & Beck, H. Activity-dependent control of neuronal output by local and global dendritic spike attenuation. *Neuron* **61**, 906–916 (2009).
- Harnett, M.T., Xu, N.-L., Magee, J.C. & Williams, S.R. Potassium channels control the interaction between active dendritic integration compartments in layer 5 cortical pyramidal neurons. *Neuron* **79**, 516–529 (2013).
- Losonczy, A. & Magee, J.C. Integrative properties of radial oblique dendrites in hippocampal CA1 pyramidal neurons. *Neuron* **50**, 291–307 (2006).
- Poirazi, P., Brannon, T. & Mel, B.W. Pyramidal neuron as two-layer neural network. *Neuron* **37**, 989–999 (2003).
- London, M. & Häusser, M. Dendritic computation. *Annu. Rev. Neurosci.* **28**, 503–532 (2005).
- Xu, N.-L. *et al.* Nonlinear dendritic integration of sensory and motor pathways produces an object localization signal. *Nature* **492**, 247–251 (2012).
- Ames, A. III & Nesbett, F.B. *In vitro* retina as an experimental model of the central nervous system. *J. Neurochem.* **37**, 867–877 (1981).
- Masland, R.H. The neuronal organization of the retina. *Neuron* **76**, 266–280 (2012).
- Wässle, H. Parallel processing in the mammalian retina. *Nat. Rev. Neurosci.* **5**, 747–757 (2004).
- Gollisch, T. & Meister, M. Eye smarter than scientists believed: neural computations in circuits of the retina. *Neuron* **65**, 150–164 (2010).
- Barlow, H.B. & Hill, R.M. Selective sensitivity to direction of movement in ganglion cells of the rabbit retina. *Science* **139**, 412–414 (1963).
- Barlow, H.B. & Levick, W.R. The mechanism of directionally selective units in rabbit's retina. *J. Physiol. (Lond.)* **178**, 477–504 (1965).
- Oyster, C.W. & Barlow, H.B. Direction-selective units in rabbit retina: distribution of preferred directions. *Science* **155**, 841–842 (1967).
- Taylor, W.R., He, S., Levick, W.R. & Vaney, D.I. Dendritic computation of direction selectivity by retinal ganglion cells. *Science* **289**, 2347–2350 (2000).
- Vaney, D.I., Sivyer, B. & Taylor, W.R. Direction selectivity in the retina: symmetry and asymmetry in structure and function. *Nat. Rev. Neurosci.* **13**, 194–208 (2012).
- Euler, T., Detwiler, P.B. & Denk, W. Directionally selective calcium signals in dendrites of starburst amacrine cells. *Nature* **418**, 845–852 (2002).
- Fried, S.I., Munch, T.A. & Werblin, F.S. Mechanisms and circuitry underlying directional selectivity in the retina. *Nature* **420**, 411–414 (2002).
- Lee, S., Kim, K. & Zhou, Z.J. Role of ACh-GABA cotransmission in detecting image motion and motion direction. *Neuron* **68**, 1159–1172 (2010).
- Briggman, K.L., Helmstaedter, M. & Denk, W. Wiring specificity in the direction-selectivity circuit of the retina. *Nature* **471**, 183–188 (2011).
- Wei, W., Hamby, A.M., Zhou, K. & Feller, M.B. Development of asymmetric inhibition underlying direction selectivity in the retina. *Nature* **469**, 402–406 (2011).
- Yonehara, K. *et al.* Spatially asymmetric reorganization of inhibition establishes a motion-sensitive circuit. *Nature* **469**, 407–410 (2011).
- Yoshida, K. *et al.* A key role of starburst amacrine cells in originating retinal directional selectivity and optokinetic eye movement. *Neuron* **30**, 771–780 (2001).
- Beier, K.T. *et al.* Transsynaptic tracing with vesicular stomatitis virus reveals novel retinal circuitry. *J. Neurosci.* **33**, 35–51 (2013).
- Koch, C., Poggio, T. & Torre, V. Nonlinear interactions in a dendritic tree: localization, timing and role in information processing. *Proc. Natl. Acad. Sci. USA* **80**, 2799–2802 (1983).
- Oesch, N., Euler, T. & Taylor, W.R. Direction-selective dendritic action potentials in rabbit retina. *Neuron* **47**, 739–750 (2005).
- Schachter, M.J., Oesch, N., Smith, R.G. & Taylor, W.R. Dendritic spikes amplify the synaptic signal to enhance detection of motion in a simulation of the direction-selective ganglion cell. *PLoS Comput. Biol.* **6**, e1000899 (2010).
- Velte, T.J. & Masland, R.H. Action potentials in the dendrites of retinal ganglion cells. *J. Neurophysiol.* **81**, 1412–1417 (1999).
- He, S., Jin, Z.F. & Masland, R.H. The nondiscriminating zone of directionally selective retinal ganglion cells: comparison with dendritic structure and implications for mechanism. *J. Neurosci.* **19**, 8049–8056 (1999).
- Rall, W. & Rinzel, J. Branch input resistance and steady attenuation for input to one branch of a dendritic neuron model. *Biophys. J.* **13**, 648–687 (1973).
- Chen, W.R., Midtgaard, J. & Shepherd, G.M. Forward and backward propagation of dendritic impulses and their synaptic control in mitral cells. *Science* **278**, 463–467 (1997).
- Stuart, G.J. & Sakmann, B. Active propagation of somatic action potentials into neocortical pyramidal cell dendrites. *Nature* **367**, 69–72 (1994).
- Brandon, C. Cholinergic neurons in the rabbit retina: dendritic branching and ultrastructural connectivity. *Brain Res.* **426**, 119–130 (1987).
- Famiglietti, E.V. Synaptic organization of complex ganglion cells in rabbit retina: type and arrangement of inputs to directionally selective and local-edge-detector cells. *J. Comp. Neurol.* **484**, 357–391 (2005).
- Murayama, M. *et al.* Dendritic encoding of sensory stimuli controlled by deep cortical interneurons. *Nature* **457**, 1137–1141 (2009).
- Lavzin, M., Rapoport, S., Polsky, A., Garion, L. & Schiller, J. Nonlinear dendritic processing determines angular tuning of barrel cortex neurons *in vivo*. *Nature* **490**, 397–401 (2012).
- Harnett, M.T., Makara, J.K., Spruston, N., Kath, W.L. & Magee, J.C. Synaptic amplification by dendritic spines enhances input cooperativity. *Nature* **491**, 599–602 (2012).
- Famiglietti, E.V. Synaptic organization of starburst amacrine cells in rabbit retina: analysis of serial thin sections by electron microscopy and graphic reconstruction. *J. Comp. Neurol.* **309**, 40–70 (1991).
- Yonehara, K. *et al.* The first stage of cardinal direction selectivity is localized to the dendrites of retinal ganglion cells. *Neuron* **79**, 1078–1085 (2013).
- Rhodes, P. The properties and implications of NMDA spikes in neocortical pyramidal cells. *J. Neurosci.* **26**, 6704–6715 (2006).
- Jadi, M., Polsky, A., Schiller, J. & Mel, B.W. Location-dependent effects of inhibition on local spiking in pyramidal neuron dendrites. *PLoS Comput. Biol.* **8**, e1002550 (2012).
- Gidon, A. & Segev, I. Principles governing the operation of synaptic inhibition in dendrites. *Neuron* **75**, 330–341 (2012).
- Williams, S.R. Spatial compartmentalization and functional impact of conductance in pyramidal neurons. *Nat. Neurosci.* **7**, 961–967 (2004).

ONLINE METHODS

Retinal preparation. Adult pigmented rabbits of either sex (Nanowie small animal production unit) were dark adapted for 1–2 h, anesthetized with ketamine (12 mg per kg of body weight, intramuscular) and xylazil (12 mg per kg, intramuscular), and overdosed with pentobarbitone sodium (150 mg per kg, intravenous) before the eyes were quickly enucleated, hemisected and placed in carbogenated Ames solution (8.9 g l⁻¹ Ames, 1.9 g l⁻¹ sodium bicarbonate, 0.7 g l⁻¹ D-glucose) at 23–24 °C. All protocols were approved by the Animal Ethics Committee of the University of Queensland. Large sections of the inferior peripheral retina were separated from the sclera and pigmented epithelial layer and stored in carbogenated Ames solution at 23–24 °C. A single section was placed in a recording chamber perfused with Ames solution at 35–37 °C.

Identification and targeting of ON-DSGCs. There are multiple classes of DSGCs in the mammalian retina²³. Both sustained ON-DSGCs and ON-OFF DSGCs receive directionally tuned GABAergic inhibition from starburst amacrine cells^{25,29–31}. We studied the integrative mechanisms of sustained ON-DSGCs because they have a unistratified dendritic tree that receives only ON excitatory inputs and lie close to the inner margin of the inner plexiform layer. ON-DSGCs were visually targeted using infrared differential interference contrast video microscopy based on soma shape, and the presence of large primary dendrites that often traversed ~100 μm laterally in the ganglion cell layer before branching in sublamina-B of the inner plexiform layer. In most experiments, a large caliber parent dendrite was followed from the soma to a distal branch point and, using a patch electrode containing Ames solution, a small hole was made in the inner limiting membrane (ILM) and the tissue around the dendrite gently removed. Following the establishment of a somatic whole-cell recording a new electrode containing internal solution was used to record from the dendrite. Once dual dendritic and somatic whole-cell recordings were established, the objective was changed from a 60× (1.0 NA, Olympus) to a 10× (0.3 NA, Olympus) for visual stimulation.

Visual stimulation and whole-cell recording. Visual stimuli were generated using custom software (developed by W.R. Taylor (Oregon Health and Sciences University) and R.G. Smith (University of Pennsylvania)) and presented on a 800 × 600 pixel OLED screen (OLED-XL microdisplay, Emagin). In most experiments, the background illumination was maintained above the level of rod saturation at $\approx 3.5 \times 10^{11}$ quanta cm⁻² s⁻¹ and the visual stimuli were set at 100% of the background (5.25×10^{11} quanta cm⁻² s⁻¹ for ON stimuli). Moving light bars (100 × 300 μm, 240 μm s⁻¹), and a range of light spot sizes (50–200 μm) focused on the photoreceptor outer segments were used to physiologically activate ON-DSGCs. Dual whole-cell recordings were made with identical current-clamp amplifiers configured in bridge mode (BVC 700A, Dagan). Voltage and current signals were low-pass filtered at DC to 10–30 kHz and sampled at 50 kHz. Recording pipettes were filled with 135 mM potassium gluconate, 7 mM NaCl, 10 mM HEPES, 10 mM phosphocreatine, 2 mM Na₂-ATP, 0.3 mM Na-GTP, 2 mM MgCl₂ and 0.35 mM Alexa Fluor 594 or 488 (Molecular Probes) (pH 7.3–7.4, KOH), and had an open tip resistance of 4–5 MΩ

for somatic and 15–20 MΩ for dendritic pipettes. ON-DSGCs were included for further analysis if the resting membrane potential at both somatic and dendritic recording sites was more negative than -50 mV. No correction was made for liquid junction potential. Dendritic current-evoked input-output relationships were constructed by the injection of repeated (50-ms interval) short (2-ms duration) current steps with a pseudo-random amplitude distribution centered around the rheobase current for dendritic spike initiation in the absence and presence of null-direction moving light bar stimuli. At the termination of each whole-cell recording the location of the recording pipettes and neuronal morphology were examined by fluorescence microscopy and digitally recorded (QImaging).

Pharmacology. TTX (1–10 μM dissolved in Ames solution) was pressure applied to the region of a small hole torn in the ILM close to the dendritic recording electrode for ~5–10 s until the initiation of dendritic spikes by step current injection or light stimuli was abolished. Recordings where TTX diffused to the axon to influence axonal action potential firing were excluded. The application of TTX to terminal dendritic sites was achieved by making a small hole in the ILM, using a patch electrode containing Ames solution, distal to the dendritic recording site, which corresponded to the location of terminal dendrites. The effect of TTX on the initiation of small-amplitude dendritic spikes was tested by the short duration (0.5–2 s) pressure application of TTX to distal dendritic sites. In each trial, the spatial extent of terminal dendritic TTX application was verified by the presentation of positive current pulses to the dendritic or somatic recording electrode to exclude the possibility that TTX had affected parent dendritic or axonal spike initiation. Gabazine (SR-95531, 10 μM, Sigma) was bath applied, or pressure applied (1–2 s) to distal dendritic sites, using methods identical to the terminal dendritic application of TTX.

Data and statistical analysis. The time-delay between simultaneously recorded regenerative events was measured at peak amplitude. For analysis of time delay as a function of visual stimulus position, regenerative events from each cell were binned according to their spike times for each segment where the moving bar (240 μm s⁻¹) traversed 20 μm of the receptive field. A direction index was calculated using the formula: (preferred action potentials – null action potentials) / preferred action potentials, where 1 would correspond with the generation of all action potentials in the preferred direction and 0 with an equal number of action potentials in both directions. Amplitude histograms were pooled from multiple cells and grouped into 1 mV bins. Temporal jitter was calculated as the s.d. of the latency of dendritic spike initiation in response to steps of positive current delivered through the dendritic recording electrode. Data sets were compared using Student's *t* test (paired, two-sided), and statistical significance accepted at *P* < 0.05. Normality of distribution was established with Kolmogorov-Smirnov test with Dallal-Wilks-Lillie post test. No statistical methods were used to predetermine sample sizes. Data collection and analysis were not randomized or performed blind to the conditions of the experiments. Numerical values are presented as mean ± s.e.m. unless otherwise stated.